Indian Journal of Engineering & Materials Sciences
Vol. 27, February 2020, pp. 87-95

Corrosion behavior of boride diffusion layer on CoCrMo alloy surface

José Luis Arguelles-Ojeda[a], Joel Moreno-Palmerin[b], Alberto Saldaña-Robles[c], Miguel Angel Corona-Rivera[d], Martin Zapata-Torres[e] & Alfredo Márquez-Herrera[c*]

[a]Mechanical Engineering and Management, COARA, Autonomous University of San Luis Potosi, San Luis Potosí, SLP 78 000, Mexico

[b]Metallurgic Engineering, Campus Guanajuato, Division of Engineering (DI), University of Guanajuato, Guanajuato, Guanajuato, 36 020, Mexico

[c]Agricultural Mechanical Engineering, Campus Irapuato-Salamanca, Life Sciences Division (DICIVA), University of Guanajuato, Irapuato, Guanajuato 36 500, Mexico

[d]Chemical Engineering, COARA, Autonomous University of San Luis Potosi, Matehuala, SLP 78 700, Mexico

[e]Instituto Politécnico Nacional, Research Center for Applied Sciences and Advanced Technology (CICATA-IPN), Mexico City 11500, Mexico

Received: 12 July 2018; Accepted:22 August 2019

In the present study, the corrosion behaviour of CoCrMo ASTM F75 alloy with boride diffusion layer and under simulated physiological conditions has been investigated using electrochemical methods. Corrosion has been analyzed using Tafel and electrochemical impedance spectroscopy (EIS) curves. The corrosion resistance optimization of boride diffusion layer on ASTM F-75 alloy using a central composite design (CCD) in response surface methodology (RSM) has been studied. A boronizing thermochemical treatment has been carried out at different temperatures, time periods and paste mass. The roughness for samples subjected to boride annealing has been higher than that of the unboride sample. X-ray diffraction (XRD) measurement has shown that the boride layer of the sample at least consists of a mixture of CoB and CrB phases. The EIS and Tafel curves results have suggested that boride ASTM F75 alloy has not been a suitable candidate for orthopedics applications.

Keywords: ASTM F-75, CoCrMo, Boriding, RSM, EIS, Tafel

1 Introduction

At present, ASTM F-75 alloy (CoCrMo) is one of the most important alloys used for orthopedics applications. Due potential toxicity of Co and Cr is a cause of concern for orthopedics applications[1], applying surface treatments to CoCrMo alloys can be useful to minimize this effect**.** Particularly, the boriding process is one of the surface treatments where the formation of boride layers is developed on the surface of ferrous and non-ferrous alloys, enhancing the mechanical and chemical properties such as hardness, wear and corrosion[2,3]. Chiefly, mechanical and corrosion properties on borided CoCrMo alloys are one of the goals that several investigations have focused in. It is important to remark that although there are several authors[4-10] that had studied the boriding on ASTM F-75 alloy surface, but they do not show if it satisfies with the requirements of biocompatibility.

The boronizing presents a diffusion penetration with an excellent adhesion bonding between diffusion layer and substrate where some attempts[2,3] have been made to decrease the corrosion rate of metals and alloys suggesting that the boride layer acts as a barrier between the metal or alloy and the corrosive fluid. Using other boronizing methods as powder-pack boriding process, powder boriding, etc.[4,5,9-11] have been reported mainly the formation of the CoB/Co_2B layers on the surface of an ASTM F-75 alloy. Additionally, the boronizing (also called boriding) process has emerged as a low-cost alternative[7,12-25], and now accepted as an excellent choice for surface hardening. This process takes the advantage of the phenomenon of diffusion of boron into the metal surface to be hardened by heating. The final boronized metal surface shows improvement in its mechanical properties such as greater hardness, better wear resistance, and greater resistance to corrosion and oxidation[18,24]. Although there are several boronizing methods[7,19-23] and many formulations[14,26-32] to produce the boride layer, this work considered boronizing process by employing a boron commercial paste. In this study the electrochemical corrosion behaviors in a Hank's solution with respect to the

*Corresponding author (E-mail: amarquez@ugto.mx)

variation in the temperature, time and mass paste conditions of boronizing process on ASTM F-75 alloy surface were examined. The corrosion data were obtained through the Tafel extrapolation and linear polarization electrochemical techniques. The corrosion resistance of boronized samples was compared with unboride sample.

2 Experimental Procedure

The boronizing process was carried out by employing the commercial Durborid boron paste (typical it consists of 5 wt% B_4C powder diluted with 90 wt% SiC of refractory material and 5 wt% KBF_4 as a flux). For thermal treatments, a conventional muffle was used. A profilometer Mitutoyo® model Surftest-310 was used to measure the mean roughness (R_a) according to ISO-4287 standard. The corrosion resistance of the boride layer was tested using a VersaStat3-500 electrochemical interface from Princeton Applied Research Inc., which contained a frequency response analyzer (FRA). Corrosion was analyzed using TAFEL and electrochemical impedance spectroscopy (EIS) curves. The X-ray diffraction (XRD) measurements were performed with a Rigaku X'pert diffractometer using the Cu$K_\alpha$line ($\lambda_{k\alpha1}$ = 1.54056 ˚A and $\lambda_{k\alpha2}$ = 1.54439 ˚A). Surface morphology was evaluated by an optical microscope and a scanning electron microscope (SEM) Jeol JSM-5300 equipped with an energy dispersive detector (EDS).

The experimental procedure of the samples was carried out in three stages: preparation of the samples, boronizing by the paste, and an analysis of the layer.

2.1 Preparation of the samples

ASTM F-75 alloy (CoCrMo) was used as a substrate (25.4 mm diameter and 4 mm thickness). The chemical composition of CoCrMo alloy has a balanced weight percentage cobalt, 28-weight percentage chromium, and 6-weight percentage molybdenum. All samples were mechanically polished using SiC sandpaper from 240 to 5000 until a mirror finishing was achieved. In order to clean the surface, the samples were washed consecutively in an ultrasonic bath with methanol, acetone, and isopropanol, and finally with deionized water; the duration of each step was 5 min.

2.2 The boronizing process by response surface methodology

Response surface methodology (RSM) was applied for the boronizing process. This methodology was used to design and optimize the boronizing process by considering three factors: temperature, time and paste quantity (mass) and constructing a prediction model for the response factors. It is important to note that for practical purposes, the mass of boron paste is reported instead of depth of paste over the surface of the samples in such a way that 30 g, 45 g and 60 g of mass paste correspond about 8 mm, 11.5 mm and 15 mm of boron paste depth, respectively. A central composite design (CCD) was used in combination with RSM to carry out the experimental study. The codec factors and the corresponding levels of the boronizing process are shown in Table 1. The experimental data were evaluated by the analysis of variance (ANOVA), using STATGRAPHICS software. The CCD experiment was performed with 17 experiments with 3 replicas (51 experiments): 8 factorial points, 6 face centered points and 3 central points (Table 2).

Each specimen was placed inside a dry pressing die of 50.8 mm diameter, and then a mass of boron paste was spread on the surface to deposit a layer to according Table 1 with 2 replicas (3 runs by condition). To enhance the contact, a load of 16 kN was applied over the pressing die for 10 min. Finally, the sample was placed and inserted inside the preheated muffle at the desired temperature and time as mentioned in Table 2.

After the boronizing process, the residual paste left on the surface was cleaned by washing the samples in

Table 1 — Codec levels of factors.

Independent variable	Factor	Codeclevels		
		–1	0	1
Temperature (°C)	T	800	900	1000
Time (h)	t	3	4	5
Paste mass (g)	m	30	45	60

Table 2 — Experimental conditions of the samples to boride.

Sample	Temperature (°C)	Time (h)	Paste mass (g)
3	1000	3	30
5		5	
12		4	45
7		3	60
10		5	
15	900	4	30
13		3	45
1, 9, 17		4	
14		5	
16		4	60
2	800	3	30
4		5	
11		4	45
6		3	60
8		5	

boiling water and then were brushed using a toothbrush. Finally, the samples were washed consecutively in the ultrasonic bath as mentioned earlier.

2.3 Analysis of layer

The corrosion study was conducted using the polarization technique (Tafel) and electrochemical impedance spectroscopy (EIS). Body fluids contain numerous products as salts, organic molecules and inorganic species where fluid properties and composition can readily change because of disease, aging and drug ingestion. To avoid any uncertainty, Hank's solution, (NaCl, 80 g/L; KCl, 4 g/L; glucose, 10 g/L; KH_2PO_4 600 mg/L; Na_2HPO_4 475 mg/L and phenol red, 170 mg/L), was used as the simulated body fluid to be used for characterizing metallic biomedical CoCrMo alloy[34]. Tafel and EIS were performed using Hank's solution in a 3-electrode flat cell kit (model K0235) at ambient temperature. An Ag/AgCl (3.5 M KCl) electrode and a platinum mesh were used as reference and counter electrode, respectively. An area of 1 cm^2 of boride alloy substrate was used as the working electrode.

Before the measurements, an open circuit potential (OCP) was applied for 60 min. OCP was made because it was not done an evolution of corrosion in samples (immersion days of the samples). OCP means that the working electrode (sample) was left for 60 minutes in contact with solution (electrolyte) without apply any potential or current to the corrosion system. Samples usually get in equilibrium in less than 60 minutes. For the impedance test, a sinusoidal AC signal of 10 mV (RMS) amplitude and sweep from 0.01 Hz to 100,000 Hz were used. Tafel plots were obtained in a single scan by beginning the scan −250 mV vs. corrosion potential, E_{corr} (cathodic Tafel plot) and scanning continuously to +250 mV vs. E_{corr} (anodic Tafel plot). A step of 1 mV every 2 s (0.5 mV/s) was used. The resulting curve is a plot of the applied potential vs the logarithm of the measured current. To determine the corrosion current (I_{corr}), a straight line was superimposed along the linear portion of the anodic or cathodic curve and extrapolated to E_{corr}. Under ideal conditions, the Tafel plot is linear over a range of potentials. For a cathodic Tafel plot, this occurs between −50 mV and −250 mV vs. E_{corr}. For an anodic Tafel plot, this occurs between +50 mV and +250 mV vs. E_{corr}. A best fit straight line is extrapolated through E_{corr}, and the point of intersection at E_{corr} gives the I_{corr} value.

The reading of the surface roughness was obtained by using the 5 μm radius diamond tip of the portable surface roughness tester of 1 mm length, at a speed of 1 mm/s, with accuracy of 0.01 μm. In the boride cross-section of the disk specimens (25.4 mm diameter and 4 mm thickness), three roughness readings were recorded for each specimen in a line along the radius of the specimen, this measurements were taken in the center, in the upper middle radius and in the lower middle radius of the disk specimen. An average final R_a of the three measurements was calculated for each test specimen, which is shown according to Table 2.

To determinate the percentage of each phase in the boride layer of sample, the quantitative phase composition was analyzed according to the rietveld refinement method[35] using the Maud software[36]. The crystal data for each phase used in the quantitative phase analysis were obtained from crystallography open database (COD)[37]. Additionally, for metallographic examination, the cross section of the optimal sample was mounted in bakelite and polished. Finally, the polished sample was etched to reveal the microstructure of the boride coating.

3 Results and Discussion

The polarization curves (Tafel), Nyquist and Bode diagrams (EIS)[38] can be used to evaluate the effect of boride layer in the corrosion resistance of ASTM F-75 alloy samples. Results obtained by EIS are presented in Fig. 1 (Nyquist plot). These results show the 17 runs considering the 2 replicas. The impedance Z is represented in the complex plane, where the real part

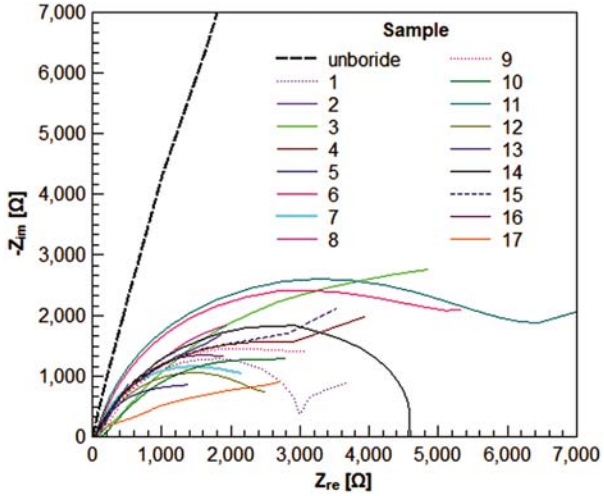

Fig. 1 — Complex impedance curves for unboride and boride samples in Hank's solution.

is plotted on the x-axis and the imaginary part on the y-axis of a chart for different frequencies. As can be clearly seen from Fig. 1, impedances of all boride samples are significantly lower than that of the unboride sample. As a first approximation, these results suggest that boride alloys are less resistant to corrosion than the unboride ASTM F-75 alloy. It could be due the corrosion resistance value associated with the oxide film and the passivation on the unboride material surface[11,39] is major than boride one.

Impedance spectra fitted parameters using the equivalent electrical circuits (EEC) given in Fig. 2 are shown in Table 3 with a relative standard error (RSE) less than 10 %.EIS spectra for unboride ASTM F-75 alloy can be represented by simple equivalent circuit shown in Fig. 2a where L and R_{sol} stands for the inductance and resistance of the electrolyte, respectively; the constant phase element, Q, and the resistor, R, may correspond to substrate[39,40]. For the boride samples, Fig. 2b, the equivalent circuit is proposed with defects[40] where R_{pore} may be the pore,

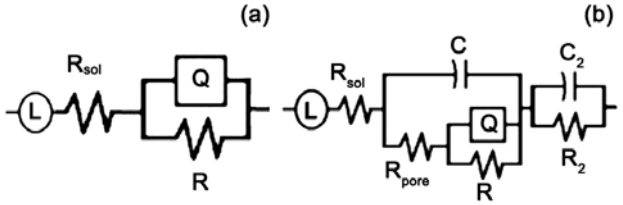

Fig.2 — Equivalent electrical circuits used to model impedance data (a) unboride ASTM F-75alloy and (b) boride ASTM F-75 alloy.

crack or roughness electrical resistance to the ionic current through the pores and the resistor, R, may correspond to boride layer. C_2 and R_2 may represent the pseudo capacitance and resistance, respectively, of the interface between the boride layer and substrate or a second layer[3,40-43].

It is noted that for almost all the samples, R_{sol} is very similar as expected since the same solution was used. The polarization resistance, R_p, is represented by the sum of the resistance of the layer, R, the pore resistance, R_{pore} and the solution resistance, R_{sol}. It is emphasized that the result of the polarization resistance, R_p, is inversely proportional to the corrosion rate, where a high R_p corresponds to a low rate of corrosion[44,45]. Table 3 shows that R_p value of unboride sample is about 930513.9 Ωcm^{-2} while R_p values greatly decrease when boronizing is applied to samples. Due R_p value is the measure of the impeded flow of ions through solutions, interfaces and layer, these results also suggest that boride ASTM F75 alloy is less resistance to corrosion than unboride sample. The EEC for the borided CoCrMo alloy (Fig. 2b) suggests porosity or cracks in the boride layer (R_{pore}), as consequence, aggressive ions can penetrate through the porosity in the layers causing corrosion of the alloy. Additionally, the corrosion resistance test of boride and unboride samples were represented by Bode plots as shown in Fig. 3.

Figure 3 shows the (a) Bode and (b) Bode phase plots of boride and unboride samples. The main effect of boride layer is a decrease in the impedance modulus, |Z|, below 100 mHz (a decrease in

Table 3 — Parameters of the proposed equivalent circuits.

Sample	L (H)	R_{sol} ($\Omega \cdot cm^2$)	C ($F \cdot cm^{-2}$)	R_{pore} ($\Omega \cdot cm^2$)	Q-Yo ($S\text{-}sec^n$)	Q-n ($0 < n < 1$)	R ($\Omega \cdot cm^2$)	C_2 ($F \cdot cm^{-2}$)	R_2 ($\Omega \cdot cm^2$)	R_p ($\Omega \cdot cm^2$)
Unboride	8.2E-5	13.9	----	---	2.3E-5	0.9	930500	---	---	930513.9
1	---	35.9	6.4E-6	14.9	3.2E-4	0.6	1802	3.9E-4	1424	3276.8
2	2.4E-5	33.8	---	----	2.1E-3	0.5	621	2.5E-3	3331	3985.8
3	---	89.8	2.6E-5	191.6	3.1E-4	0.6	9904	1.7E-5	20.8	10206.2
4	1.9E-5	34.5	1.0E-4	54.2	6.4E-4	0.7	4551	2.4E-5	9.7	4649.4
5	2.8E-5	30.0	5.9E-4	18.1	2.3E-3	0.7	4788	1.5E-4	6.4	4842.5
6	---	32.2	2.9E-5	5.7	9.8E-4	0.6	6876	5.6E-4	282.8	7196.7
7	2.2E-5	32.2	3.3E-4	42.3	1.8E-3	0.8	3037	5.7E-5	11.3	3112.8
8	3.1E-5	28.4	7.7E-6	85.4	7.8E-5	0.6	705	7.1E-6	8.79	827.8
9	---	37.8	1.1E-4	89.7	1.0E-3	0.7	4451	1.7E-5	21.9	4600.4
10	---	148.3	4.6E-5	2.2	1.1E-3	0.6	5102	5.8E-3	533	5785.5
11	1.9E-5	33.0	1.1E-5	7.4	5.2E-4	0.6	6080	2.0E-4	3112	9232.4
12	6.3E-5	15.9	1.1E-4	69.8	7.2E-4	0.7	3065	6.0E-5	11	3161.7
13	2.9E-5	30.7	1.2E-3	34.5	3.7E-3	0.7	2377	3.9E-4	4.7	2446.9
14	1.4E-5	36	7.0E-6	18.5	1.3E-4	0.7	2300	1.9E-4	2363	4717.5
15	5.4E-5	19	1.4E-4	71.9	2.1E-3	0.7	5213	2.5E-5	18	5321.9
16	5.7E-5	18	8.3E-5	76.9	7.5E-4	0.7	4024	1.8E-5	20	4138.9
17	3.2E-5	30.8	---	---	4.9E-4	0.5	3658	2.3E-5	148.5	3837.3

polarization resistance (R_p)) and a lower phase angle, Fig. 3b. These results also suggest that boride ASTM F75 alloy is less resistance to corrosion than unboride sample. Moreover, Fig. 3b shows the presence of up to two-time constants in some of the boride samples. The time constant at high frequencies could be related to the outer boride layer while the second time constant, at low frequencies, could be associated with the inner boride layer or all layer but more work is needed. By other hand, Fig. 4 shows the Tafel curves of unboride and boride samples. The values of corrosion potential (E_{corr}) and corrosion current (I_{corr}) obtained from the polarization curves by the Tafel extrapolation method are shown in Table 4.

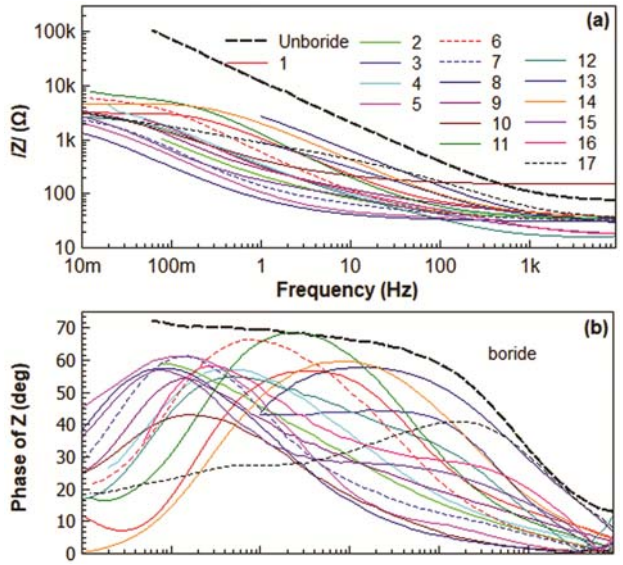

Fig. 3 — Bode plots in Hank's solutions of unboride and boride samples.

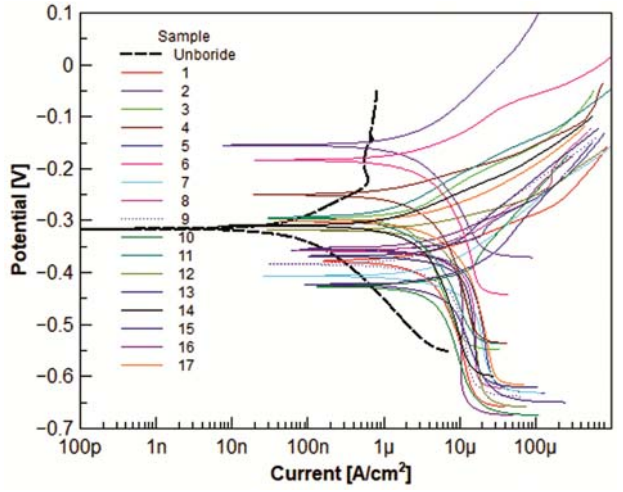

Fig. 4 — Tafel curves in Hank's solutions of unboride and boride alloy.

It is important to note that the last data was analyzed by RSM, but its adjusted R^2 statistic was not acceptable[46], perhaps because more factors need to be considered than those indicated in Table 1. Table 4 shows that the charge exchange activity (I_{corr}) at the interface for the samples subjected to boride annealing is higher than that of the unboride sample; this manifest itself as an increase in the corrosion current, I_{corr}. By contrast, these results suggest that the boride diffusion layer do not protect the alloy from chemical reaction of ions. It is noted that this result is consistent with that proposed by G. Rosas-Becerra *et al.*[11] and contrary as insinuate by other authors[4-10]. From this, it can be concluded that during the boronizing kinetics of our samples, resistance to corrosion decreases independent of temperature, paste mass and time used. The samples that have the most negative E_{corr} can present some extra protection, even having a higher I_{corr} than the unboride sample, acting as cathodic protection to the ASTM F75.

There are different parameters which can affect electrochemical reactions such as type of electrolyte, velocity, temperature, oxidizing agents, impurities, anode material type and surface treatment, but surface roughness is an important influence on general corrosion[47]. In this sense, surface roughness measurements were carried out on all the boride samples and the results were compared with unboride one. The analysis of variance (ANOVA) for the roughness (R_a) was carried out after normalizing the data (Table 5).

Table 4 — Summary of results obtained from corrosion tests performed in Hank's solution.

Sample	E_{corr} (mV)	I_{corr} (µA)	χ^2
Unboride	-316.266	0.081	3.29
1	-378.946	4.870	28.47
2	-155.536	4.644	18.60
3	-296.863	5.186	54.36
4	-250.551	2.346	52.16
5	-358.346	9.009	24.70
6	-184.494	3.859	10.16
7	-407.486	9.157	31.70
8	-359.084	16.533	26.69
9	-383.975	3.396	16.01
10	-427.665	5.142	14.61
11	-294.603	1.121	43.26
12	-319.386	3.872	22.07
13	-424.851	10.610	44.57
14	-310.170	2.579	36.61
15	-368.830	6.436	34.97
16	-353.996	3.744	26.75
17	-302.810	6.873	21.57

The R^2 = 0.776 indicates that the model as fitted explains 77.6 % of the variability in roughness. The adjusted R^2 statistic is 73.1 %. The standard deviation of the residuals to be 0.06. The mean absolute error (MAE) of 0.04 is the average value of the residuals. The Durbin-Watson (DW) statistic = 2.07424 (P = 0.5870) and since the P-value is greater than 5.0 %, there is no indication of serial autocorrelation in the residuals at the 5.0 %significance level. ANOVA results in Table 5 indicate temperature and time factors are the most significant parameter. Linear effect of paste mass is a statistic insignificant parameter. Except the interactions among temperature and time, and pasta mass and time factors, all the quadratic terms appear to be significant. Eq. (1) shown the regression model applied to the experimental data to predict the value of roughness (R_a) at the different values of the factors employed. Temperature (T), paste mass (m) and time (t) were used as the parameters to model R_a. This expression is

$$R_a = 6.01359 - 0.0105073T - 0.0196534m - 0.494678t + 0.00000542723T^2 + 0.0000427778Tm - 0.0000583333Tt - 0.000210642m^2 - 0.000111111mt + 0.060939t^2 \quad \ldots (1)$$

Fig. 5 contains information about values of roughness generated using the fitted model, Eq. (1) and 95.0 % confidence limits for the mean response.

The effect of the temperature and time, keeping constant the paste mass, is shown in Fig. 5. It shows the response surface for R_a indicating the mean roughness value (R_a) in the experimental region. It can be realized that a higher temperature and lower time results in a considerable increase in boride surface roughness, but even with that Fig. 5 shows that the roughness for any sample subjected to boride annealing is higher than that of the unboride sample. Also, this could be because the surface degradation in boride sample caused an increase in roughness and therefore a larger surface area compared with that of that unboride sample. Clearly, boride samples have larger surface area to react with ions even under unboride sample and perhaps results in a higher corrosion current with respect to unboride sample. From this, it can be partly concluded that during the boronizing kinetics of our samples, resistant to corrosion decreases independent of time, temperature and paste mass may be due roughness, too.

In this sense, X-ray characterization of some samples was carried out. Fig. 6 shows the X-ray diffractogram of the samples, subjected to the thermochemical hardening with boron, using 45 g of paste mass, a duration of 4 h and varying the temperature from 850 °C to 1000 °C. The strong and sharp diffraction peaks further affirm the crystalline nature of the boride layer. The result of the Rietveld refinement of boride samples, with an adjust factor R_{WP} better than 10 %, using 45 g of paste mass, a duration of 4 h and varying the temperature from 850 °C to 1000 °C is reported in Table 6. It is important to note

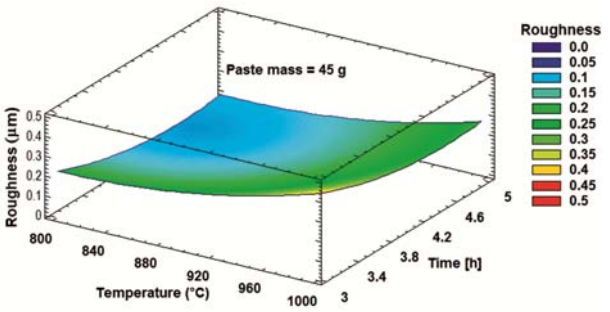

Fig. 5 — Three-dimensional plot of surface roughness.

Table 5 — Analysis of variance for roughness.

Source	Sum ofsquares	DF	Mean square	F-ratio	P-value
T: Temperature	0.272653	1	0.272653	66.69	0.0000
m: Paste mass	0.00208333	1	0.00208333	0.51	0.4794
t: Time	0.125453	1	0.125453	30.68	0.0000
TT	0.023675	1	0.023675	5.79	0.0207
Tm	0.0988167	1	0.0988167	24.17	0.0000
Tt	0.000816667	1	0.000816667	0.20	0.6573
mm	0.0180546	1	0.0180546	4.42	0.0418
mt	0.0000666667	1	0.0000666667	0.02	0.8990
tt	0.0298486	1	0.0298486	7.30	0.0100
Total error	0.167629	41	0.00408851		
Total (corr.)	0.750169	50			

DF = degrees of freedom; F-ratio = test statistic; P-value = observed significance applicable only within the experimental region; the magnitudes of the variables are specified in their original units.

that Rietveld refinement was running using all possible phases that could be found in boron paste and alloy and also formed by the reaction of boron with elements in alloy and only was found the formation of borides (CoB and CrB) in the surface. In this sense, the positions of the diffraction peaks associated with the crystal structure of CoB, CrB, Co and Cr were obtained from 96-900-8946, 96-900-8949, 96-901-1617 and 96-901-1599 card of the powder diffraction files (PDF) database, respectively.

Also, it is important to remark that a major temperature of 1000 °C is difficult to reach in the lab, but also it is not well applicable for industrial processing. Table 6 shows that the percentage of phases found in the boride layer is almost constant until 950 °C. When temperature is 1000 °C, the boride layer presents an abrupt increment of CoB and a decrement of CrB phase percentage. These results show that there are abrupt or discrete phase changes in the material during certain boring process conditions and in some cases, it could even cause that R^2 value is not acceptable when RSM is used. This could be due to RSM adjusting a curve considering continuous changes but what happens in the boriding process is that these changes are discrete, as can be seen in Table 6. This may explain the reason why almost all authors do not use RSM in thermal treatments as discussed in a previous paper[48]. In addition, these results suggest that RSM should be used with care when it involves the phases in materials.

The X-ray results suggest that during the annealing process, B_4C becomes unstable and the boron atom is liberated, and then it diffuses into the material surface reacting with Co and Cr forming the phases of CoB and CrB.

Additionally, the metallographic characterization of boride samples using 45 g of paste mass, a duration of 4 h and varying the temperature from 850 °C to 1000 °C shown in Fig. 7 was carried out. Also, Table 7 shows the thickness of boride layers. Fig. 7 displays the microstructure of the layer formed on the surface of the boride CoCrMo alloy. At least three remarkable zones were revealed: the outer and inner layer, maybe CrB and CoB layers, and a noteworthy diffusion zone. It is important to note that although the micrographs in Fig. 7 is very similar to that reported by others works[4,5,7,11], however the phases found are different, perhaps because another CoCr alloy, source of boron or conditions were used. Also it could be due an inadequate or insufficient experimental analysis, for example: Campos-Silva *et al.*[4] reported that boriding

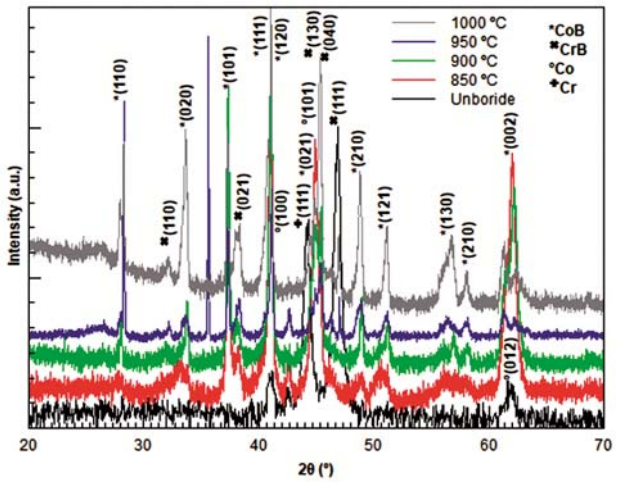

Fig. 6 — X-ray diffractograms of the samples using 45 g of paste mass, a duration of 4h and varying the temperature from 850 °C to 1000 °C.

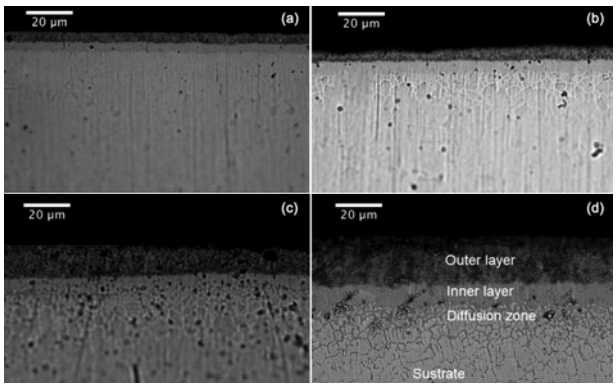

Fig. 7 — Cross sectional metallographic view of boride samples using 45 g of paste mass, a duration of 4 h and temperature of (a) 850 °C, (b) 900 °C, (c) 950 °C and 1000 °C.

Table 6 — Percentage of phases found in the unboride and boride layers from Rietveld refinement.

Sample / Phase (PDF)	Unborided	850 °C	900 °C	950 °C	1000 °C
Co (96-901-1617)	39.3 ± 0.1	---	---	---	---
Cr (96-901-1599)	60.7 ± 3.9	---	---	---	---
CrB (96-900-8949)	---	45.6 ± 2.8	42.3 ± 2.7	44.7 ± 1.7	25.3 ± 0.1
CoB (96-900-8946)	---	54.4 ± 2.8	57.7 ± 2.5	57.7 ± 2.5	74.7 ± 0.8
R_{wp}(%)	3.73	6.2	6.2	6.6	3.7
R_b (%)	2.96	3.5	3.4	3.5	2.6
R_{exp}(%)	2.99	1.6	1.9	1.9	1.6

causes the formation of the CoB/Co_2B coating on the surface of an ASTM F-75 alloy but any experimental evidence was shown, only references to other authors; Others authors[5,9,10,11] shown X-ray diffractograms without a success full indexing solution or using any powder diffraction file (PDF) database. Fig. 8 displays the cross-sectional SEM view of a boride CoCrMo alloy using 52.2 g of paste mass, a duration of 4 h and a temperature of 1000 °C.

Particularly, Fig. 8 shows the four points where EDS analysis was made in the cross-sectional SEM view of boride CoCrMo: (a) the dark outer layer; the (b) dark and (c) light inner layer; and (d) diffusion zone. Because the boron cannot be quantified by this technique, the analysis is only limited to Co, Cr and Mo as shown in Table 8. Table 8 shows that the layers have different chemical compositions

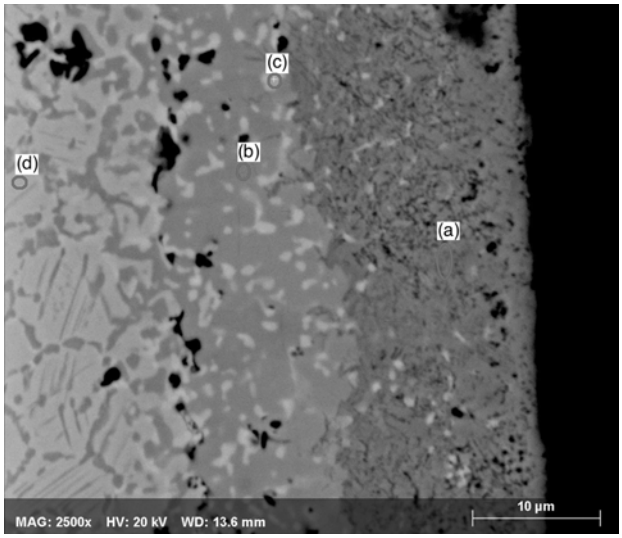

Fig. 8 — Cross sectional SEM view of the optimal boride CoCrMo alloy.

Table 7 — Thickness of boride layers using 45 g of paste mass, a duration of 4 h and varying the temperature from 850 °C to 1000 °C.

Temperature (°C)	Thickness(μm)
850	8.1 ± 0.3
900	11.0 ± 0.7
950	19.5 ± 1.4
1000	31.0 ± 1.3

Table 8 — EDS analysis made in the cross-sectional view of boride CoCrMo.

Zone in Fig. 8	Cr	Co	Mo
(a)	31.4	64.9	3.7
(b)	31.9	67.2	0.9
(c)	25.5	57.6	16.9
(d)	21.8	75.7	2.5

of Co, Cr and Mo and it suggests that there may be more phases present on the surface of the material, but more work is needed. Also, the formation of these phases could be the cause that some boride samples present E_{corr} more negative and others less negative than unboride as shown Table 4 and Fig. 4.

4 Conclusions

The polarization curves (Tafel), Nyquist and Bode diagrams (EIS) were used to evaluate the effect of boride layer in the corrosion resistance of ASTM F-75 alloy and the Response surface methodology (RSM) was applied to optimize the boronizing process. Although, it was not possible to model the effect of mass of paste, time and temperature variables on the corrosion resistant by RSM, to according the parameters used in this experiment, the boride ASTM F75 alloy presented less corrosion protection than samples with boride diffusion layer. Hence, resistant to corrosion of boride samples decrease independent of mass of paste, time and temperature used. The corrosion resistance values of CoCrMo alloy were ranged to 930513.9 $\Omega \cdot cm^{-2}$ while the corrosion resistance values estimated for the boride CoCrMo alloy were established between 827.8 $\Omega \cdot cm^{-2}$ to 10206.2 $\Omega\ cm^{-2}$.

Boride samples have larger surface area to react with ions even under unboride sample and perhaps results in a higher corrosion current with respect to unboride sample.

Additionally, X-ray diffraction study confirm that the boride layers present the CoB and CrB phases. Also, the microstructure of the layer formed on the surface of the boride CoCrMo alloy shown three remarkable zones: the outer and inner layer, and a noteworthy diffusion zone.

Acknowledgements

This work was partially supported by Laboratorio Nacional de Investigación y Desarrollo Tecnológico de Recubrimientos Avanzados (LIDTRA-LICAMM) of Cinvestav-UG.

References

1 Milosev I, Strehblow H H, *Electro Chimica Acta,* 48 (2003) 2767.

2 Márquez-Herrera A, Bermúdez-Rodríguez G, Hernández-Rodríguez E N, Melendez-Lira M & Zapata-Torres M, *Int J Mater Res,* 107 (2016) 676.

3 Márquez-Herrera A, Fernandez-Muñoz J L, Zapata-Torres M, Melendez-Lira M & Cruz-Alcantar P, *Surf Coat Technol,* 254 (2014) 433.

4 Campos-Silva I, Bravo-Bárcenas D, Meneses-Amador A, Ortiz-Dominguez M, Cimenoglu H, Figueroa-López U & Andraca-Adame J, *Surf Coat Technol,* 237 (2013) 429.
5 Mu D, Shen B I & Zhao X, *Mater Des,* 31 (2010) 3933.
6 Mu D & Shen B I, *Int J Refract Metals Hard Mater,* 28 (2010) 424.
7 Johnston J M, Jubinsky M & Catledge S A, *Appl Surf Sci*, 328 (2015) 133.
8 Metikos-Hukovíc M, Pilíc Z, Babic R & Omanovíc D, *Acta Biomater*, 2 (2006) 693.
9 Rodriguez-Castro G A, Reséndiz-Calderon C, Jiménez-TinocoL, Meneses-Amador A, Gallardo-Hernandez E A & Campos-Silva I E, *Surf Coat Technol,* 284 (2015) 258.
10 Campos-Silva I, Bravo-Bárcenas D, Cimenoglu H, Figueroa-López U, Flores-Jiménez M & Meydanoglu O, *Surf Coat Technol*, 260 (2014) 362.
11 Rosas-Becerra G, Mejía-Caballero I, Martínez-Trinidad J, Palomar-Pardavé M, Romero-Romo M, R. Pérez-Pasten-Borja R & Campos-Silva I, *J Mater Eng Perform*, 26 (2017) 704.
12 Balusamy T, Narayanan T S, Ravichandran K, Park I S & Lee M H, *Vacuum*, 97 (2013) 36.
13 Kulka M, Makuch N, Dziarski P, Miko-lajczak D & Przestacki D, *Opt Lasers Eng*, 67 (2015) 163.
14 Campos I, Palomar-Pardavé M, Amador A, Villa-Velázquez C & J. Hadad, *Appl Surf Sci*, 253 (2007) 9061.
15 Kayali Y, Gunes I & Ulu S, *Vacuum*, 86 (2012) 1428.
16 Kayali Y & Anaturk B, *Mater Desi*, 46 (2013) 776.
17 Joshi A A & Hosmani S S, *Mater Manuf Process*, 29 (2014) 1062.
18 Keddam M & Chegroune R, *Appl Surf Sci*, 256 (2010) 5025.
19 Kusmanov S, Tambovskiy I, Sevostyanova V, Savushkina S & Belkin P, *Surf Coat Technol,* 291 (2016) 334.
20 Piasecki A, Kulka M & Kotkowiak M, *Tribology Int*, 97 (2016) 173.
21 Zuno-Silva J, Ortiz-Domínguez M, Keddam M, Elias-Espinosa M, Damián-Mejía O, Cardoso-Legorreta E & Abreu-Quijano M, *J Mining Metallur. Section B: Metallur*, 50 (2014) 101.
22 Kartal G, Timur S, Sista V, Eryilmaz O & Erdemir A, *Surf & Coatings Technol*, 206 (2011) 2005.
23 Lomovsky O, Golubkova G, Bulina N, Yadroitsev I & Smurov I, *Inorganic Mater*, 49 (2013) 564.
24 Tabur M, Izciler M, Gul F & Karacan I, *Wear*, 266 (2009) 1106.
25 Xiao B, Xing J, Ding S & Su W, *Physica B: Condensed Matter*, 403 (2008) 1723.
26 Gunes I & Kanat S, *Protect Metal & Physi Chemist Surf,* 51 (2015) 842.
27 Ozdemir O, Usta M, Bindal C &Ucisik A H, *Vacuum*, 80 (2006) 1391.
28 Gunes I, Erdogan M & Celik A G, *Mater Res*, 17 (2014) 612.
29 Jiang J, Wang Y, Zhong Q, Zhou Q & Zhang L, *Surf Coat Technol*, 206 (2011) 473.
30 Baglyuk G, Mamonova A, Pyatachuk S & Sosnovskiy L, *Powder Metallu Metal Ceramics,* 52 (2013) 113.
31 Sahin S & Meric C, *Mater Res Bulletin,* 37 (2002) 971.
32 Gunes I &*Sadhana*, 38 (2013) 527.
33 William M, Jonathan B&, Garth H, *Handbook of Biomaterial Properties* (Springer Science & Business Media, USA), 2016, 159.
34 Moreto-Aparecido J, Rodrigues-Costa A, Leite-Rodrigues-da-Silva R, Rossi A, Silva-da L A & Alves-Almeida V, *Mater Res*, 21 (2018) 1.
35 Rietveld H, *Acta Crystallographica,* 22 (1967) 151.
36 Lutterotti L, Bortolotti M, Ischia G, Lonardelli I & Wenk H Z, *Kristallogr Suppl, 26* (2007) 125.
37 Merkys A, Vaitkus A, Butkus J, Okulic-Kazarinas M, Kairys V & Grazulis S, *J appl crystallo*, 49 (2016) 292.
38 Mejía-Caballero I, Palomar-Pardavé M, Trinidad J M, Romero-Romo M, Pasten-Borja R P,Lartundo-Rojas L, López-García C & Campos-Silva I, *Surf Coat Technol,* 280 (2015) 384.
39 Milosev I & Strehblow H H, *Electro Chemica Acta*, 48 (2003) 2767.
40 Carlos V V & Anna I M, *Electrochemical aspects in biomedical alloy characterization: Electrochemical impedance spectroscopy,* Edited by Anthony N L (InTech Publisher, London) (2011) 283.
41 Mansfeld F, Kendig M & Tsai S, *Corros*, 38 (1982) 478.
42 Gerengi H, *Protect of Metals Physi Chemi Surf,* 54 (2018) 536.
43 Marion M, Monica A F L M ,Wolf-Dieter M, *Adv Eng Mater,* 10 (2008) 33.
44 Wang B, Xue W, Wu J, Jin X,Hua M & Wu Z, *J Alloys Comp*, 578 (2013) 162.
45 Stern M & Geary A L, *J Electrochem Soc,* 104 (1957) 56.
46 Saldaña-Robles A, Plascencia-Mora H, Aguilera-Gómez E, Saldaña-Robles A, Márquez-Herrera A & Diosdado-De la Peña J A, *Surf Coat Technol,* 339 (2018) 191.
47 Alisina T, Vesselin S & Derek N, *Proceedings ASME Int Mech Eng Cong Expos, Volume 2B: Advanced* (2013) 15.
48 Arguelles-Ojeda J, Márquez-Herrera A, Saldana-Robles A, Saldana-Robles A, Corona-Rivera M A & Moreno-Palmerin J, *Revista Mexicana de Física,* 63 (2017) 76.